HETEROCYCLES, Vol. 102, No. 1, 2021, pp. 44 - 68. © 2021 The Japan Institute of Heterocyclic Chemistry
Received, 28th September, 2020, Accepted, 5th November, 2020, Published online, 13th November, 2020
DOI: 10.3987/COM-20-14355

SYNTHESIS, STRUCTURES, AND INTERACTIONS WITH CT-DNA/BSA OF THREE NEW ACYLHYDRAZONES CONTAINING OXAZOLE RING

Lingling Chang,[a] Xiangrong Liu,[a,b*] Zaiwen Yang,[a,b] Shunsheng Zhao,[a,b] Xinjuan Chen,[b] and Bosen Dai[b]

[a]College of Chemistry and Chemical Engineering, Xi'an University of Science and Technology, Xi'an 710054, China. [b]Key Laboratory of Coal Resources Exploration and Comprehensive Utilization, Ministry of Nature Resources, Xi'an 710021, China. E-mail: liuxiangrongxk@163.com

Abstract – Three new acylhydrazones containing oxazole ring $C_{11}H_8N_3O_2X$ (X = F, **1**; Br, **2**; I, **3**) have been synthesized. The single crystal XRD presented that **1** belonged to the monoclinic system, while **2** and **3** belonged to the triclinic systems. TG-DTG results showed that the maximum thermal decomposition temperatures of **1**-**3** were more than 260 °C. The UV-vis spectra, fluorescence spectra and microcalorimetry measurements indicated that each acylhydrazone bound to calf thymus DNA (CT-DNA) *via* groove binding mode and interacted with bovine serum albumin (BSA) by static quenching effect and the corresponding interaction processes were all exothermic. The molecular docking showed that each acylhydrazone bound to CT-DNA and BSA mainly through hydrogen bonding. The minimum inhibitory concentrations of **1**-**3** against *Escherichia coli*, *Staphylococcus aureus*, *Bacillus subtilis*, and *Pseudomonas aeruginosa* were all about 0.25 $mg \cdot mL^{-1}$.

INTRODUCTION

Acylhydrazones had attracted much attention in the fields of chemistry and biology because their unique structure units (-CONHN=CH-) were similar to the biological active group (-CONH-).[1] Acylhydrazone ligands possessing oxygen and nitrogen atoms had special strong binding abilities with proteins and deoxyribonucleic acids.[2] A large number of literature had reported that acylhydrazones had great potential as drugs with antibacterial,[3] antitumor,[4] antitubulin,[5] antioxidant,[6] and insecticidal activities.[7]

Oxazole and its derivatives were a class of five-membered aromatic rings containing nitrogen and oxygen atoms. They were able to bind with a variety of enzymes and receptors in biological systems and

exhibited versatile biological activities.[8] Hence, oxazole-based compounds displayed extensively potential applications in medicine, agriculture, and chemistry as well as material science.[9,10] Zahanich *et al*.[11] synthesized phenoxymethyl-1,3-oxazoles and 1,2,4-oxadiazoles and found that these compounds exhibited significant anticancer activities on GPR40 receptor with EC50 value of 0.058 μM. Patil *et al*.[12] introduced oxazole into 1,2,3-triazole ring, and found that the antibacterial activities of this compound against *Porphyromonas gingivalis* and *Streptococcus gordonii* increased significantly.

DNA played an important role in replication, transcription and mutation of genes. In the study of anticancer activities for drug molecules, DNA was often used as one of the main targets of anticancer drugs.[13] The interactions of drug molecules with DNA could change the replication of DNA and prevent the division of cancer cells, eventually lead to cell death.[14] Therefore, the interactions between drug molecules and DNA had been widely concerned in the life science. BSA, the most abundant protein in the circulatory system, was the transport carriers of various exogenous and endogenous compounds. The interactions of drug molecules with BSA could form stable complexes, which affected the distribution, metabolism, and efficacy of drugs in the blood stream.[15] Thus, it was important to investigate the binding behaviors of BSA with small molecules.

Based on the above facts, acylhydrazones and compounds containing oxazole ring all had strong biological activities, so in this study, we introduced oxazole rings into acylhydrazones and synthesized three new compounds, hoping to obtain the superposition of the biological activities of the two substances. The compositions and structures of all acylhydrazones were characterized by melting point test, elemental analysis, IR spectra, ^{1}H NMR and single crystal X-ray diffraction. The thermal stabilities of the acylhydrazones were analyzed by thermogravimetry. The interactions of the acylhydrazones with CT-DNA and BSA were studied by UV-vis spectra, fluorescence spectra, microcalorimetry measurements, and molecular docking studies. The antioxidant activities of the acylhydrazones were determined by DPPH radical scavenging assay. The antibacterial activities of the acylhydrazones against *Escherichia coli*, *Staphylococcus aureus*, *Bacillus subtilis*, and *Pseudomonas aeruginosa* were studied by agar diffusion test under strict aseptic conditions.

RESULTS AND DISCUSSION

We have synthesized three new acylhydrazones containing oxazole ring $C_{11}H_8N_3O_2X$ (X = F, **1**; Br, **2**; I, **3**) by the dehydration condensation reactions of the 4-oxazolecarboxylic acid hydrazides with benzaldehydes containing halogen atoms in EtOH. The reactions of titled acylhydrazones were shown in **Scheme 1**.

The synthetic routes of the titled acylhydrazones were shown in **Scheme 2**. Firstly, 4-oxazolecarboxylic acid hydrazides were prepared by the reactions of ethyl oxazole-4-carboxylate with hydrazine hydrate at

25 °C for 1 h in 85.2% yield. Next, the reactions of 4-oxazolecarboxylic acid hydrazides with three benzaldehydes containing halogen atoms were conducted in EtOH at 75 °C for 4 h under stirring conditions to produce three new acylhydrazones containing oxazole ring. **1**, **2**, and **3** were obtained in 78.8%, 84.8%, and 77.9% yields, respectively.

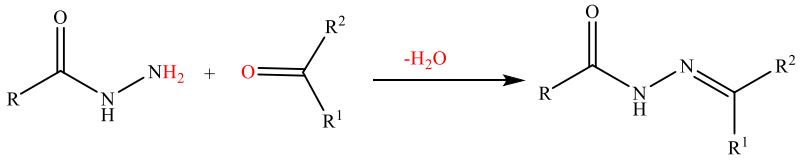

Scheme 1. The synthesis of titled acylhydrazones

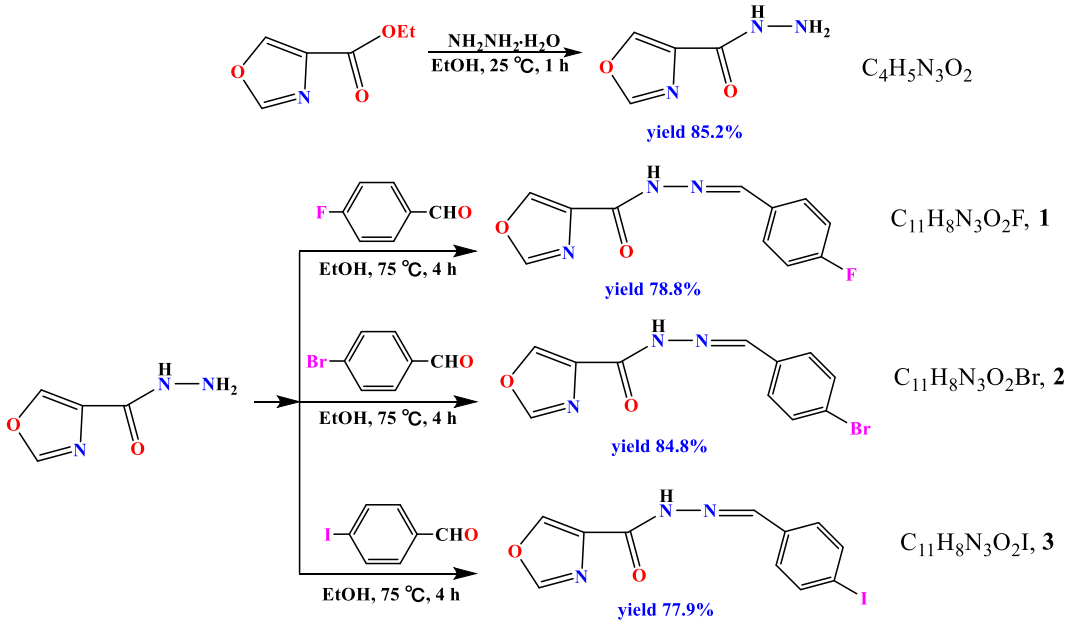

Scheme 2. The synthetic routes of the titled acylhydrazones

Crystal structure

The molecular structures of three acylhydrazones **1-3** were illustrated in **Figure 1**. The packing structures of **1-3** were displayed in **Figure 2**. The crystal data of **1-3** were given in **Table 1**, and the selected bond lengths and angles were listed in **Table 2**. The parameters of π-π stacking interactions of **1-3** were summarized in **Table 3**. As given in **Table 1**, **1** belonged to the monoclinic system and $P2_1$ space group, while **2** and **3** belonged to the triclinic systems, and $P1$ and $P\text{-}1$ space groups, respectively.

As presented in Table 2, the bond lengths of O(2)-C(4) for **1**, **2**, and **3** were 1.212(8) Å, 1.217(15) Å, and 1.228(5) Å and their bond lengths were similar to the typical C=O (1.210 Å). The bond lengths of N(3)-C(5) for **1**, **2**, and **3** were 1.280(12) Å, 1.244(15) Å, and 1.274(6) Å, respectively, which were comparable to typical C=N bond length (1.273 Å). These data showed each acylhydrazone existed in the

form of ketone.[16] The dihedral angles of the oxazole rings and the benzene rings in **1**-**3** were 26.403°, 5.718°, and 2.006°, respectively, indicating that oxazole rings and benzene rings of all acylhydrazones were not in exact parallel planes. Moreover, the torsion angles of three acylhydrazones N(3)-C(5)-C(6)-C(7) were -168.9(8), 8(2), and 174.7(4), respectively, showing that there were twists between N(3)-C(5) and benzene rings. The three acylhydrazones were expanded into 3D networks through a series of π-π stacking interactions.

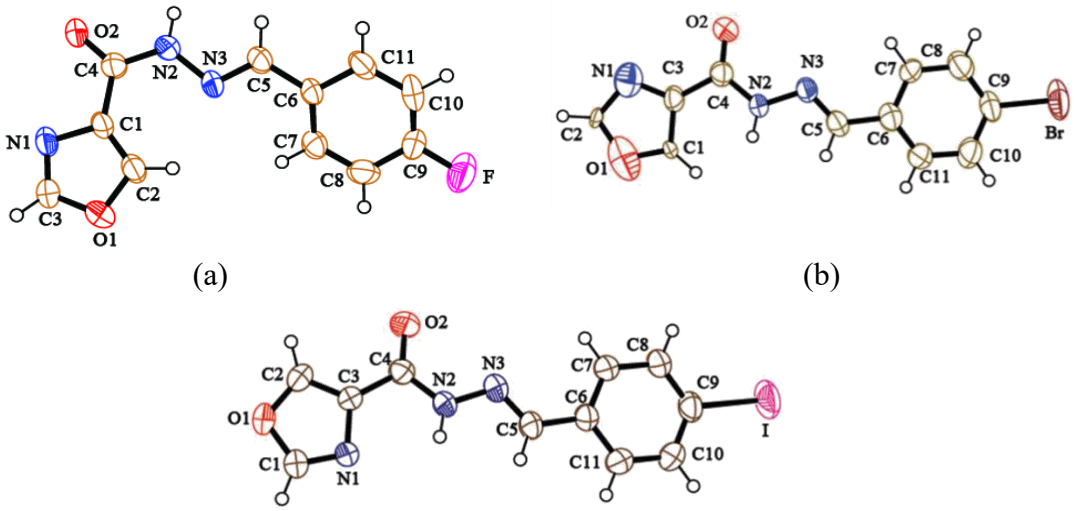

Figure 1. Molecular structures of **1**-**3**. (a) **1**, (b) **2**, (c) **3**

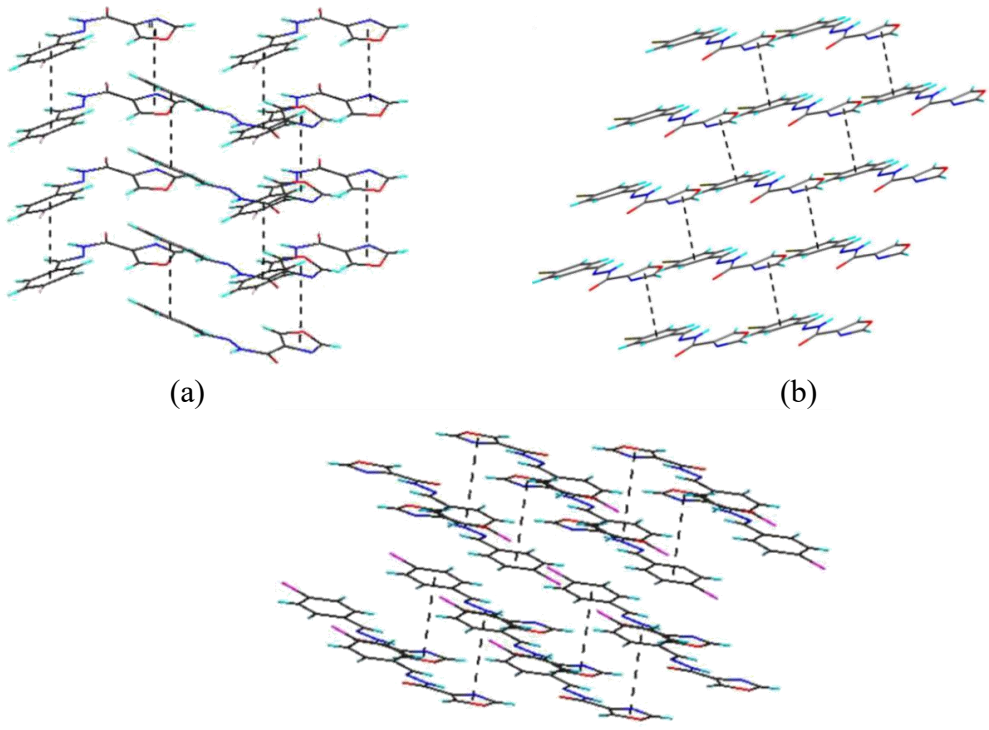

Figure 2. Crystal packing structures of **1**-**3**. (a) **1**, (b) **2**, (c) **3**

Table 1. Crystallographic data of **1**-**3**

	$C_{11}H_8N_3O_2F$ (**1**)	$C_{11}H_8N_3O_2Br$ (**2**)	$C_{11}H_8N_3O_2I$ (**3**)
CCDC number	1837875	1843541	1843542
Formula weight	233.20	294.11	341.10
Crystal system	Monoclinic	Triclinic	Triclinic
Space group	$P2_1$	$P1$	P-1
a(Å)	3.734(3)	5.270(5)	5.2795(11)
b(Å)	10.914(10)	7.532(7)	7.7035(15)
c(Å)	12.505(11)	15.029(14)	15.583(3)
α(°)	90.00	96.555	77.233
β(°)	90.175	100.021	80.340
γ(°)	90.00	107.665	73.227
V(Å^3)	508.2(8)	550.8(9)	588.1(2)
Z	2	2	2
D_c(g/cm^3)	1.524	1.773	1.926
F(000)	240	292	328
θ Range	2.48-25.10	1.40-25.10	1.35-25.10
T/K	296(2)	296(2)	296(2)
Final R indices	R_1 =0.0800	R_1 = 0.1279	R_1 = 0.0416
[I>2sigma(I)]	wR_2 = 0.1859	wR_2 = 0.3423	wR_2 = 0.1390

Table 2. Main selected bond lengths (Å), angles (°) and torsion angles (°) for **1**-**3**

Bond	**1**	**2**	**3**
X(1)-C(9)	1.339(9)	1.864(11)	2.083(5)
N(1)-C(1)	1.268(10)	1.344(17)	1.362(5)
N(2)-C(4)	1.351(11)	1.343(15)	1.349(6)
N(3)-C(5)	1.280(12)	1.244(15)	1.274(6)
O(2)-C(4)	1.212(8)	1.217(15)	1.228(5)
N(3)-N(2)-C(4)-O(2)	-179.0(7)	0.1(19)	-3.8(6)
C(1)-O(1)-C(2)-C(3)	2.7(11)	-0.2(14)	0.7(5)
C(6)-C(7)-C(8)-C(9)	3.1(14)	-2(2)	-2(2)
C(7)-C(8)-C(9)-C(10)	-1.6(14)	0(2)	0.0(8)
C(8)-C(9)-C(10)-C(11)	-0.1(13)	2(2)	-0.9(8)
C(9)-C(10)-C(11)-C(6)	0.3(13)	-1(2)	0.6(7)
C(2)-O(1)-C(1)-N(1)	2.7(11)	-1.6(15)	-1.1(5)
C(3)-N(1)-C(1)-O(1)	0.8(9)	1.0(14)	-0.8(5)
C(2)-O(1)-C(1)-N(1)	-2.2(11)	-1.6(15)	0.1(5)
C(3)-C(4)-N(2)-N(3)	6.7(11)	-176.5(11)	-174.9(4)
N(3)-C(5)-C(6)-C(7)	-168.9(8)	8(2)	174.7(4)
C(4)-N(2)-N(3)-C(5)	-174.7(8)	175.8(10)	176.2(4)

Remark: X=F(**1**), Br(**2**), I(**3**)

Table 3. Parameters of π-π stacking interactions of **1**-**3**

Compound	π-π interaction	Centroid-centroid separation (Å)	Dihedral angle (°)	Horizontal displacements between ring centroids (Å)	Vertical displacements between ring centroids (Å)
1	i	3.734(3)	0.000	1.445, 1.448	3.443, 3.442
	ii	3.734(3)	0.000	1.747, 1.758	3.300, 3.294
2	i	3.756(5)	6.314	1.716, 1.340	3.341, 3.509
3	i	3.781(7)	6.178	1.625, 1.260	3.414, 3.565

Thermal stabilities of 1-3

Figure 3 showed thermogravimetry differential thermogravimetry curves of acylhydrazones **1**-**3** under nitrogen at heating rates of 5.00, 10.00, and 15.00 °C·min^{-1}. There was only one stage of the thermal decomposition for each acylhydrazone. The maximum thermal decomposition temperatures of **1**-**3** were

all more than 260 °C at heating rate of 5.00 °C·min^{-1}, showing that all acylhydrazones had good thermal stabilities.

The apparent activation energies (E_a) of the thermal decomposition stages of **1-3** were calculated by equation (7) and equation (8) and the results were listed in **Table 4**. The apparent activation energies (E_a) of **1-3** were 79.67, 67.33, 44.97 kJ·mol^{-1} (Kissinger), 84.86, 72.88, 51.85 kJ·mol^{-1} (Ozawa), respectively. The order of apparent activation energies **1**>**2**>**3** indicated that **1** was the stablest, because the bond length of **1** was the shortest, and **1** needed to absorb the most energies in the thermal decomposition processes.

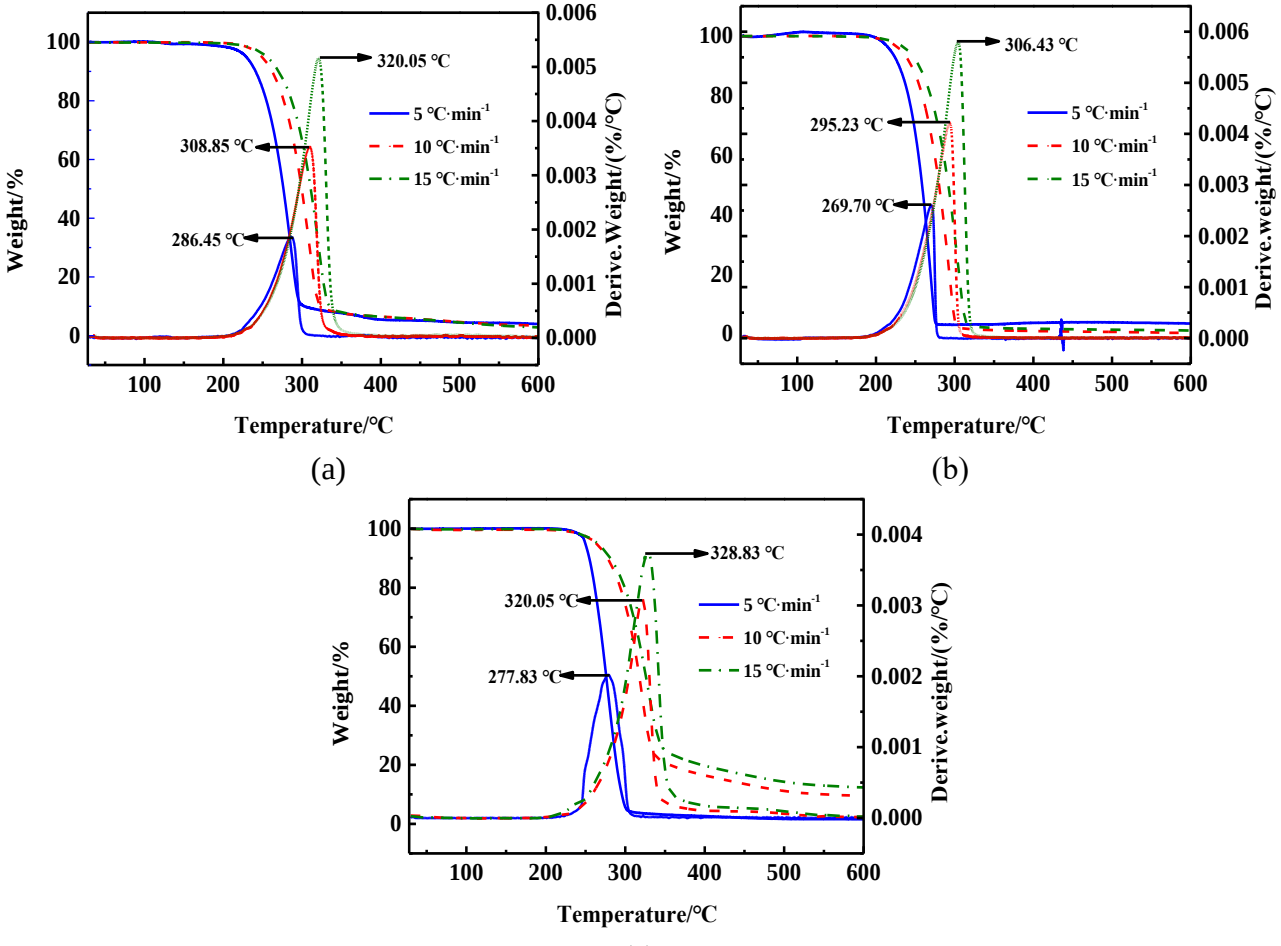

Figure 3. TG-DTG curves of **1-3** at three heating rates. (a) **1**, (b) **2**, (c) **3**

Table 4. Kinetic parameters of thermal decomposition processes for **1-3** at three heating rates

Compound	β/°C·min^{-1}	T_P/°C	Kissinger			Ozawa	
			E_a/kJ·mol^{-1}	lg$A$	r	E_a/kJ·mol^{-1}	r
1	5	286.45	79.67	4.839	-0.9982	84.86	-0.9985
	10	308.85					
	15	320.05					
2	5	269.70	67.33	3.832	-0.9953	72.88	-0.9963
	10	295.23					
	15	306.43					
3	5	277.83	44.97	1.426	-0.9642	51.85	-0.975
	10	320.05					
	15	328.83					

UV-vis absorption assay

Figure 4 was the UV-vis spectra of the interactions of **1-3** with CT-DNA. With the increase of CT-DNA concentration, the absorption bands of **1-3** exhibited a downward trend, but there were no obvious red shifts. These results indicated that each acylhydrazone bound to CT-DNA through groove binding,[17] which was due to π~π* intercoupling between the π* empty orbit of each acylhydrazone and the π orbit of CT-DNA base pairs after acylhydrazone entered into CT-DNA.[18]

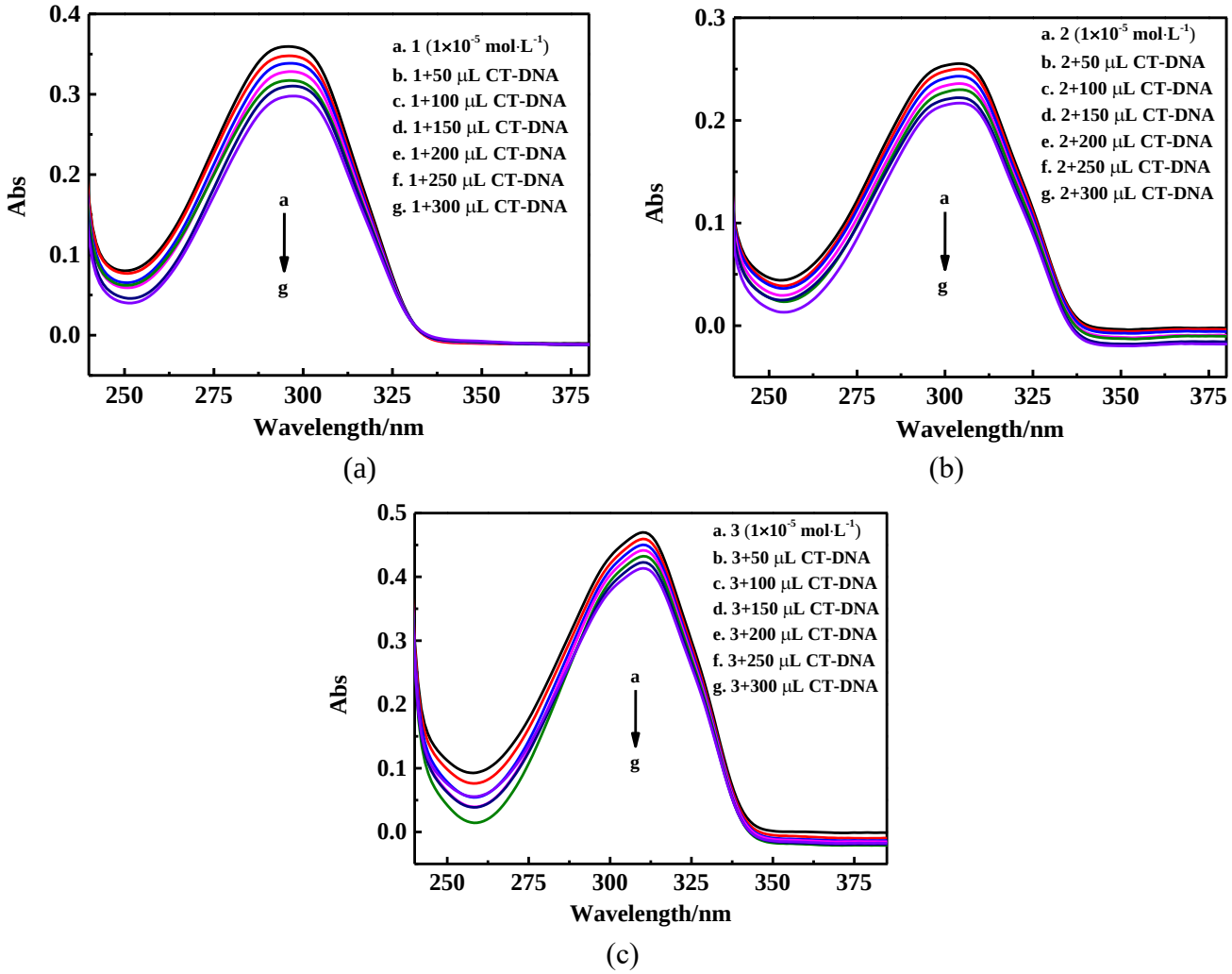

Figure 4. UV-vis absorption spectra of the interactions of **1-3** with CT-DNA. (a) **1**, (b) **2**, (c) **3**

To determine and compare the binding ability of each acylhydrazone with CT-DNA, the binding constant K_b was calculated by equation (1) and the formula was as follows.[19]

$$[\text{CT-DNA}]/(\varepsilon_a - \varepsilon_f) = [\text{CT-DNA}]/(\varepsilon_b - \varepsilon_f) + 1/[K_b(\varepsilon_b - \varepsilon_f)] \quad (1)$$

Where [CT-DNA] is the concentration of CT-DNA, K_b the binding constant of each acylhydrazone with CT-DNA, ε_a the apparent extinction coefficient of the acylhydrazone in presence of CT-DNA, ε_b the extinction coefficient of acylhydrazone that fully binds to CT-DNA and ε_f the extinction coefficient of

free acylhydrazone. ε_a, ε_b, and ε_f can be obtained by $\varepsilon = A/CL$. A the absorbance value, C the concentration, and L the absorption path (1 cm). K_b values for **1-3** were obtained from plots of [CT-DNA]/(ε_a-ε_f) against [CT-DNA] (supplementary **Figure S1**), and which were (7.64 ± 0.06)×10^5, (9.50 ± 0.06)×10^5, and (7.07 ± 0.06)×10^5 L·mol^{-1}, respectively. The order of binding constants **2>1>3** showed that the binding ability of **2** with CT-DNA was the strongest.

Fluorescence quenching studies

Fluorescence emission spectra of **1-3** interacting with ethidinium bromide and calf thymus DNA (EB-CT-DNA) were shown in **Figure 5**. As shown in **Figure 5**, with the increase of acylhydrazone concentrations, the maximum absorption intensities of EB-CT-DNA systems at about 596 nm insignificant decreased, indicating that the microenvironment of EB-CT-DNA did not change significantly and the primary binding modes of acylhydrazones with CT-DNA were groove binding.[20] The fluorescence quenching data were evaluated by the Stern-Volmer equation (2).[21]

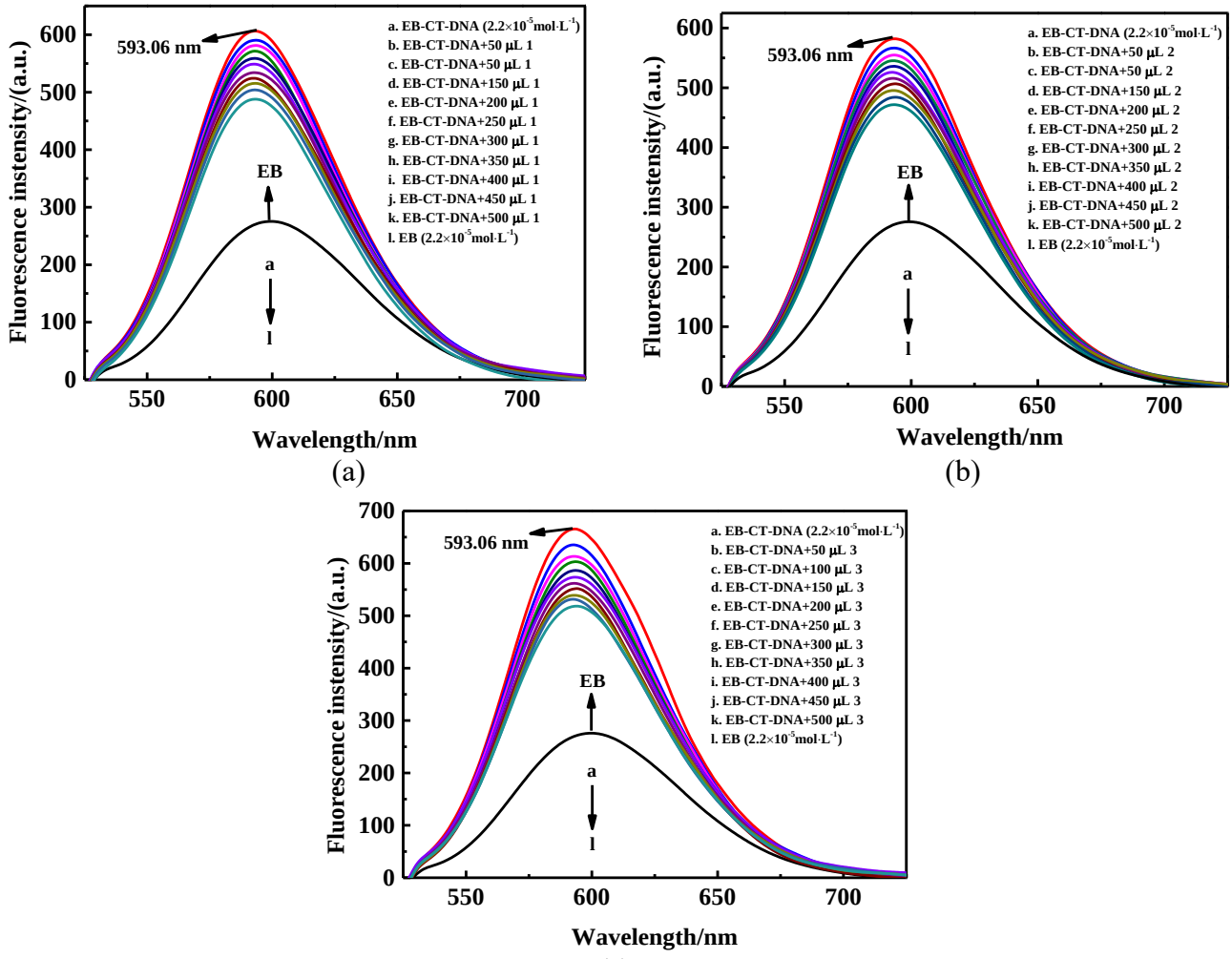

Figure 5. Fluorescence emission spectra of **1-3** interacting with EB-CT-DNA. (a) **1**, (b) **2**, (c) **3**

$$F_0 / F = K_q \tau_0 [Q] + 1 = 1 + K_{sv}[Q] \qquad (2)$$

Where [Q] is the concentration of acylhydrazone, F_0 and F the fluorescence intensities in the absence and presence of the quencher, respectively, K_{sv} the dynamic quenching constant, K_q the quenching rate constant and τ_0 (10^{-8} s) the fluorescence lifetime.

Supplementary **Figure S2** was plots of the F_0/F against [Q] of the **1-3**. K_q values of **1-3** were given by the slopes from the plots of F_0/F against [Q] and they were (2.19 ± 0.05)×10^{11}, (2.51 ± 0.05)×10^{11}, and (2.10 ± 0.08)×10^{11} L·mol^{-1}, respectively. K_q Values for **1-3** were larger than the maximum diffusion collision quenching rate constant (2.0×10^{10} L·mol^{-1}·s^{-1}),[22] showing that the quenching mechanism was static quenching rather than dynamic quenching. The above data revealed that all acylhydrazones could bind to CT-DNA and **2** had the strongest binding ability with CT-DNA.

Microcalorimetry measurements

Figure 6 displayed the thermogenic curves of **1-3** interacting with CT-DNA at 25 °C. The thermogenic curves of the interaction of **1-3** with CT-DNA started at 3.96, 3.02, and 2.89 min and ended at 45.06, 48.27, and 53.74 min, respectively. The reaction times of **1-3** interacting with CT-DNA were all less than 51 min. As shown in **Figure 6**, the enthalpy changes (ΔH) of the reactions between acylhydrazones and CT-DNA were obtained by integral heat flux curves and were listed in **Table 5**. The processes of **1-3** interacting with CT-DNA were all exothermic. The absolute values of ΔH for **1-3** were all beyond 3.0×10^3 kJ·mol^{-1} and the order of ΔH was **2>1>3**, showing that **2** had the strongest binding ability with CT-DNA, which was consistent with the results of UV-vis absorption assay. ΔS and ΔG could be obtained by the thermodynamic equations (3) and (4), and the formulas were as follows.

$$\Delta G = -RT\ln K \qquad (3)$$

$$\Delta S = (\Delta H - \Delta G)/T \qquad (4)$$

Where ΔG refers to Gibbs function change, ΔS the entropy change, ΔH enthalpy change, K binding constant of each acylhydrazone with CT-DNA (K_b), K_b comes from equation (3). T the temperature in Kelvin and R the gas constant.

The values of ΔH, ΔG, and ΔS were listed in **Table 5**. As seen from **Table 5**, the values of ΔG, ΔS, and ΔH for **1-3** were all less than 0, indicating the interactions of **1-3** with CT-DNA were spontaneous exothermic and entropy reduction processes.

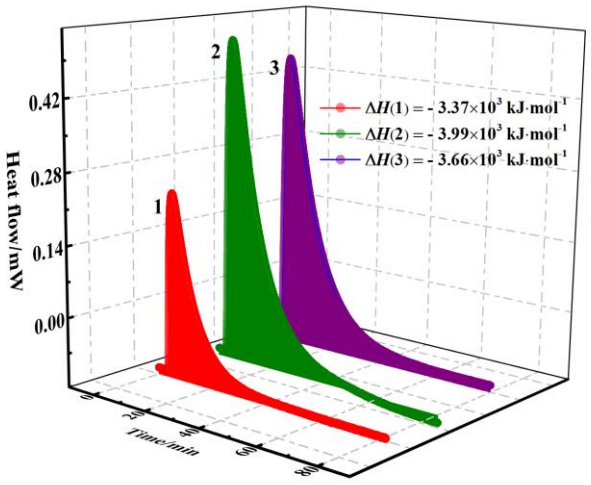

Figure 6. Thermogenic curves of **1-3** interacting with CT-DNA

Table 5. Thermodynamic parameters of the interactions of **1-3** with CT-DNA

Compound	ΔG (kJ·mol^{-1})	ΔS (kJ·mol^{-1}·K^{-1})	ΔH (kJ·mol^{-1})	Start time (min)	End time (min)	Reaction time (min)
1	-33.57	-12..40	-3.73×10^3	2.89	53.74	50.85
2	-34.12	-13.26	-3.99×10^3	3.02	48.27	45.25
3	-33.39	-12.16	-3.66×10^3	3.96	45.06	41.10

Molecular docking with DNA

Molecular docking was used to further confirm the binding locations and mechanisms of **1-3** interacting with CT-DNA. The best docked poses of **1-3** in the binding sites of DNA and detailed views of binding modes of **1-3** with DNA were shown in **Figures 7-9**. As can be seen from **Figures 7-9**, indicating the groove binding mode of DNA with **1-3**. For **1**, N2-H2 group and N3-H3 group of **1** formed two hydrogen bonds with O atoms in DT6 and DC20. N2-H2 group in **2** interacted with O atom of DC21 to form one hydrogen bond and the hydrophobic interactions were observed between **2** and DA7 and DC21. N1-H1 group and N2-H2 group in **3** exhibited two hydrogen bonds with N atom and O atom of DT18 and DG16, respectively. Besides, there were some hydrophobic interactions between **3** and DT18 and DG10. The binding energy values of **1-3** interacting with DNA were -5.87, -6.47, and -5.23 kcal·mol^{-1}, respectively, indicating that **2** had the strongest ability to interact with DNA.

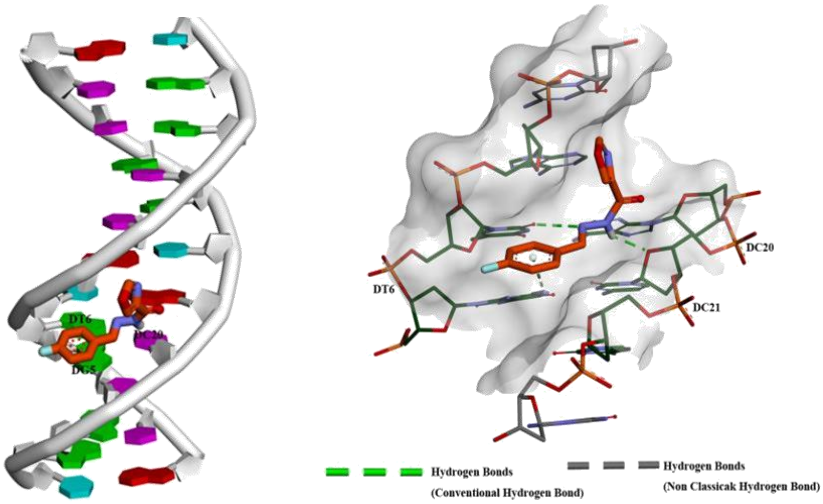

(a) (b)

Figure 7. Molecular docking result of **1** with DNA (a) The best docked pose of **1** in DNA (b) Detailed view of binding mode of **1** with DNA

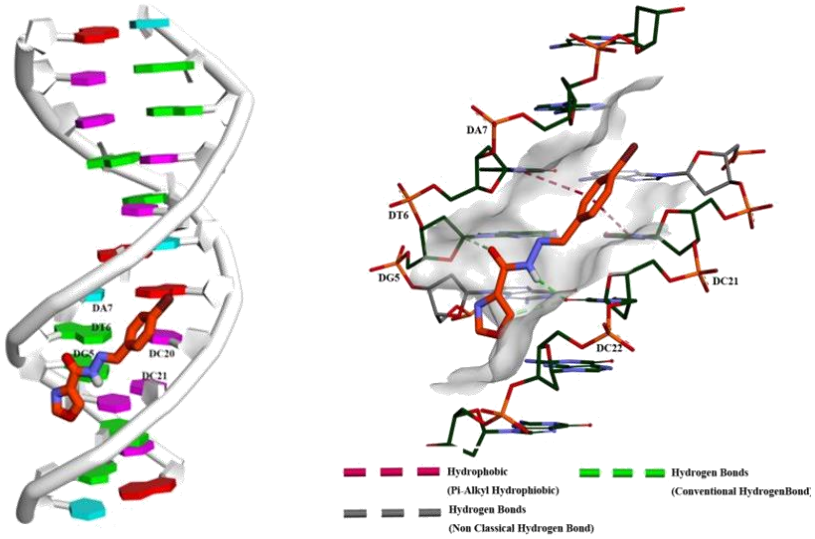

(a) (b)

Figure 8. Molecular docking result of **2** with DNA (a) The best docked pose of **2** in DNA (b) Detailed view of binding mode of **2** with DNA

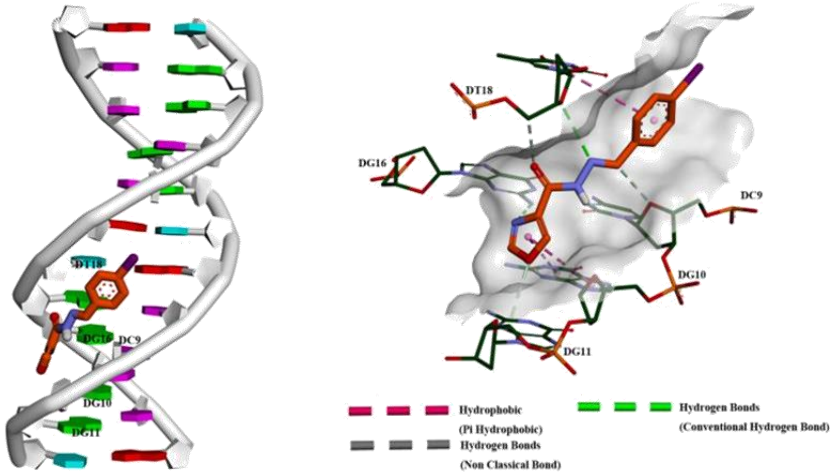

(a) (b)

Figure 9. Molecular docking result of **3** with DNA (a) The best docked pose of **3** in DNA (b) Detailed view of binding mode of **3** with DNA

BSA binding studies

UV-vis absorption spectral studies

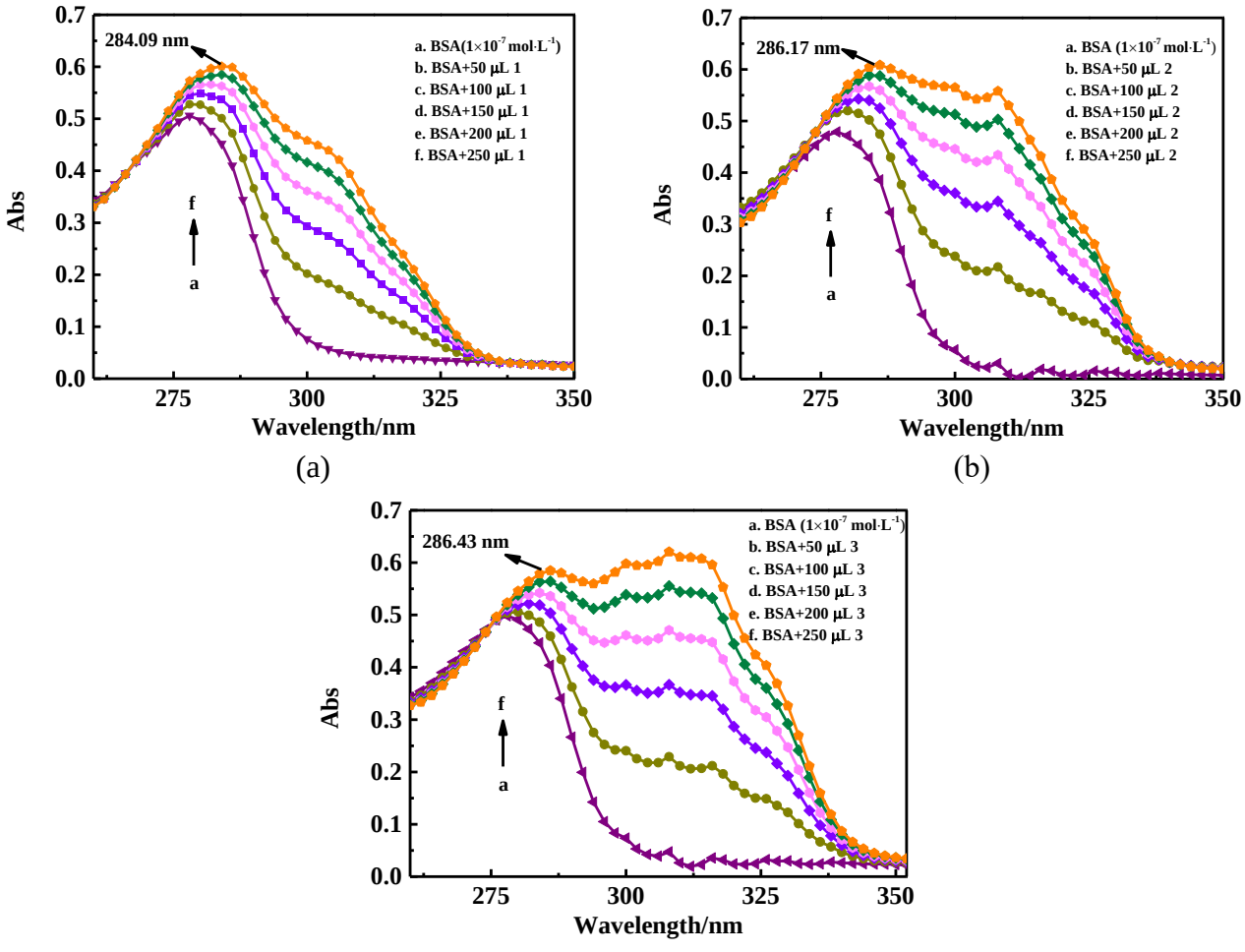

(a) (b)

(c)

Figure 10. UV-vis absorption spectra of the interactions of **1**-**3** with BSA. (a) **1**, (b) **2**, (c) **3**

The UV-vis spectra of the interactions of **1-3** with BSA were shown in **Figure 10**. As the acylhydrazone concentration was increased, the intensity of absorption band of each acylhydrazone at about 286 nm was increased and shifted toward longer wavelength. The above phenomena indicated that microenvironment of BSA was changed. The formation of non-fluorescence ground-state complex of BSA and acylhydrazone induced the change in absorption spectra of fluorophore, speculating the quenching mechanism of BSA with each acylhydrazone was static quenching.[23]

Fluorescence quenching studies

In order to eliminate the inner filter effects of BSA and **1-3**, the following equation (5) was used to correct the fluorescence intensity and avoid re-absorption and inner filter effects.[24]

$$F_{obs} = F_{corr} \times 10^{-\frac{A_{ex} \times d_{ex}}{2} - \frac{A_{em} \times d_{em}}{2}} \qquad (5)$$

Where F_{obs} is the observed fluorescence intensity, F_{corr} the correct fluorescence intensity, d_{ex} and d_{em} the cuvette pathlengths in the excitation and emission direction (1 cm), respectively, and A_{ex} and A_{em} the absorbance values at the excitation and emission wavelengths, respectively.[25]

The fluorescence emission spectra of the interaction of **1-3** with BSA were shown in **Figure 11**. As presented in **Figure 11**, a significant decrease in the fluorescence intensity of each acylhydrazone was observed at about 340 nm along with small blue shift with increasing acylhydrazone concentration, which indicated that each acylhydrazone interacted with BSA. The Stern-Volmer equation (2) and equation (6) could be used to describe this combination process.[26]

$$\log[(F_0 - F)/F] = \log K_A + n\log[Q] \qquad (6)$$

Where $[Q]$ is the concentration of the acylhydrazone, F_0 and F the fluorescence intensities in the absence and presence of the quencher, respectively, n the number of binding sites and K_A the binding constant.

According to equation (4), the values of K_q for **1-3** were obtained and listed in **Table 6**. They were bigger than the maximum diffusion collision quenching rate content (2.0×10^{10} L·mol^{-1}·s^{-1}),[27] indicating that the quenching process of BSA bound with **1-3** was static quenching rather than dynamic quenching. Supplementary **Figure S3** showed the plots of $\log[(F_0\text{-}F)/F]$ versus $\log[Q]$. The values of K_A, n and R^2 were calculated and listed in **Table 6**. The value of each n was close to 1, indicating that there was only one binding site between BSA and each acylhydrazone. As we all known, there were two tryptophan residues processed intrinsic fluorescence of BSA, and one was TRP213 and another was TRP134. The intrinsic fluorescence of BSA mainly came from TRP213, because TRP134 was more exposed to hydrophilic environment and its fluorescence quenched by H_2O molecule.[28] Therefore, the single binding site indicated that **1-3** most likely to interacted with BSA through the hydrophobic cavity near TRP213.[29]

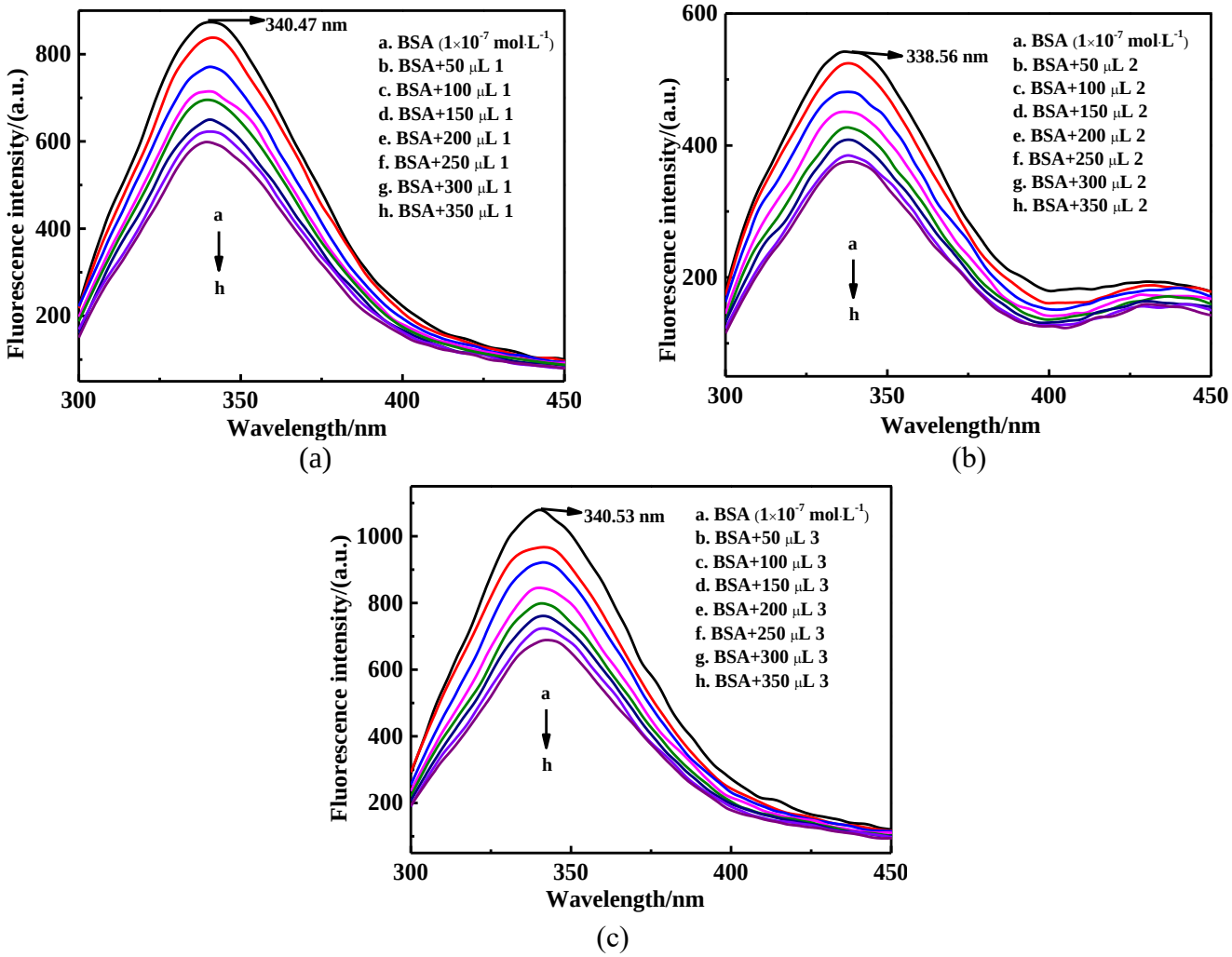

Figure 11. Fluorescence emission spectra of the interactions of **1-3** with BSA

Table 6. Fluorescence quenching parameters of the interactions of **1-3** with BSA

Compound	K_q/L·mol^{-1}·s^{-1}	K_A/L·mol^{-1}	n	R^2
1	6.83×10^{11}	$(4.09 \pm 0.34)\times10^{3}$	1.2307	0.97035
2	6.85×10^{11}	$(1.06 \pm 0.40)\times10^{4}$	1.3552	0.98165
3	7.63×10^{11}	$(1.13 \pm 0.15)\times10^{3}$	1.0360	0.99181

Microcalorimetry measurements

Figure 12 showed the thermogenic curves of **1-3** interacting with BSA at 25 °C. The thermogenic curves of the interaction of **1-3** with BSA started at 2.29, 2.02, and 2.29 min, and ended at 39.25, 45.78, and 34.13 min, respectively. The reaction times of **1-3** interacting with BSA were all less than 44 min and the processes of **1-3** interacting with CT-DNA were exothermic. As shown in **Figure 12**, the enthalpy changes (ΔH) of the reactions between acylhydrazones and BSA were obtained by integral heat flux curves and found to be -3.73×10^3, -3.99×10^3, and -3.66×10^3 J·mol^{-1}, respectively. The absolute values of ΔH for **1-3** were all beyond 6.0×10^3 kJ·mol^{-1} and the value of ΔH(**2**) reached 4 order of magnitude,

indicating that the binding ability of **2** interacting with BSA was the strongest, which was consistent with the results of fluorescence spectra. The values of ΔS and ΔG could be obtained by the thermodynamic equations (3) and (4). K was binding constant (K_A) of each acylhydrazone with BSA and they were obtained by equation (6). The values of ΔH, ΔG, and ΔS were listed in **Table 7**. As seen from **Table 7**, $\Delta G<0$, $\Delta S<0$, and $\Delta H<0$, indicating the interactions of **1-3** with BSA were spontaneous exothermic and entropy reduction processes.

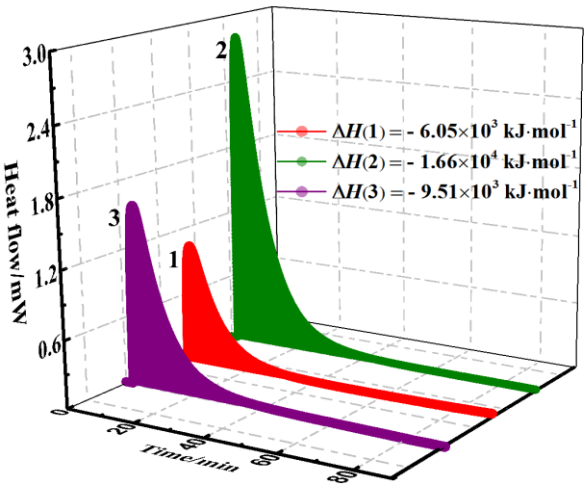

Figure 12. Thermogenic curves of **1-3** interacting with BSA

Table 7. Thermodynamic parameters of the interactions of **1-3** with BSA

Compound	ΔG (kJ·mol^{-1})	ΔS (kJ·mol^{-1}·K^{-1})	ΔH (kJ·mol^{-1})	Start time (min)	End time (min)	Reaction time (min)
1	-20.61	-20.22	-6.05×10^3	2.29	34.13	31.84
2	-22.98	-55.60	-1.66×10^4	2.02	45.78	43.76
3	-17.43	-31.84	-9.51×10^3	2.29	39.25	36.96

Molecular docking with BSA

The best docked poses of **1-3** in the binding sites of BSA and detailed views of binding modes of **1-3** with BSA were illustrated in **Figures 13-15**. As presented in **Figures 13-15**, **1-3** docked in the hydrophobic cavity near TRP213, which confirmed the results of fluorescence quenching experiment. N-H groups of VAG347 and VAL481 formed two hydrogen bonds with O2 atoms of **1** and O-H groups of ARG347 and ARG484 formed two hydrogen bonds with N1 and N3 atoms of **1**. Moreover, there were also some hydrophobic interactions between **1** and LEU346, LEU197, LEU456, and ARG484. For **2**, N2-H2 group interacted with O atom of ALA209 to form one hydrogen bond and VAL481, ALA212, ALA209, TRP213, ARG198, and LEU 197 were involved in hydrophobic contacts with **2**. There was a halogen bond between Br and ARG194. For **3**, N2-H2 group in **3** exhibited a hydrogen bond with oxygen atom of

ALA209. In addition, the hydrophobic interactions were observed between **3** and LEU197, ARG198, TRP213, and ALA212. There was also a halogen bond between I atom of **3** and ARG194. The binding energy values of **1**-**3** with BSA were -5.30, -6.16, and -5.35 kcal·mol^{-1}, respectively, indicating that **2** had the strongest ability to interact with BSA.

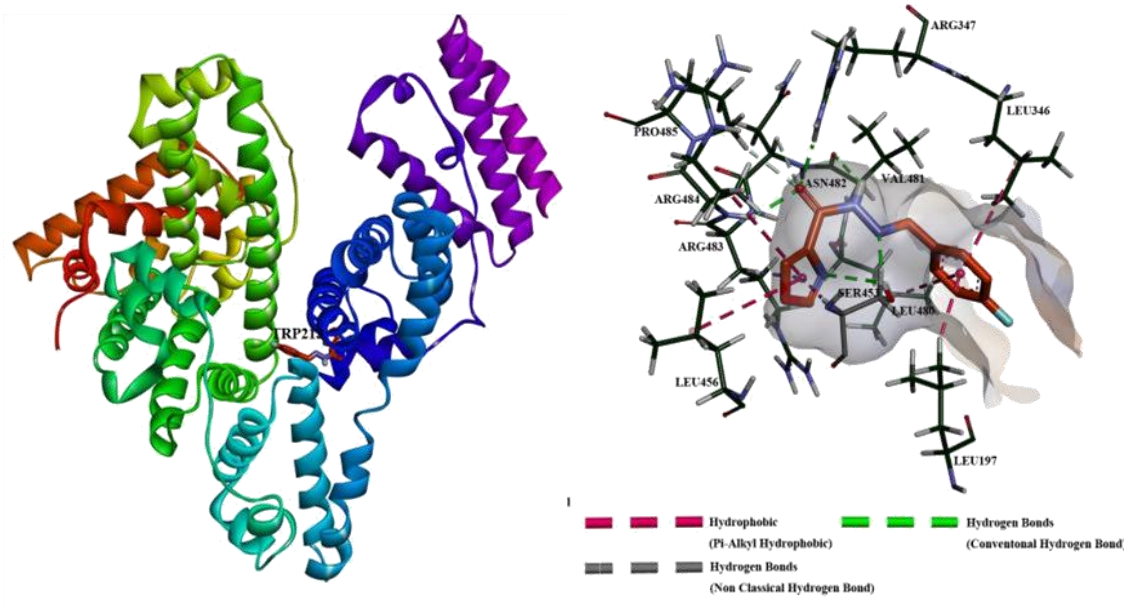

(a) (b)

Figure 13. Molecular docking result of **1** with BSA (a) The best docked pose of **1** in BSA (b) Detailed view of binding mode of **1** with BSA

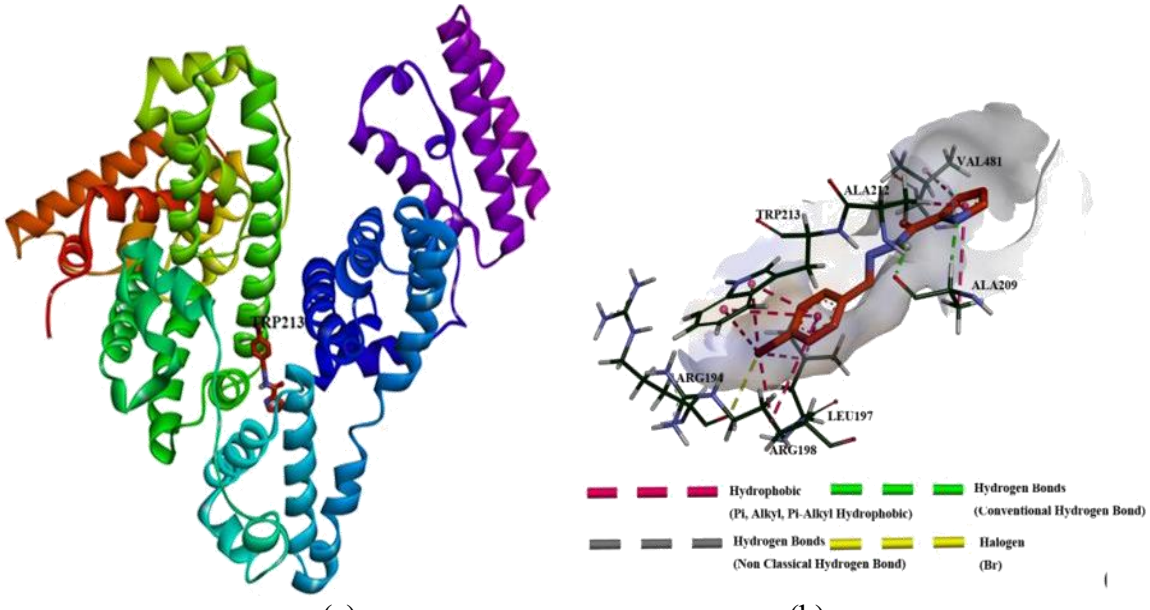

(a) (b)

Figure 14. Molecular docking result of **2** with BSA (a) The best docked pose of **2** in BSA (b) Detailed view of binding mode of **2** with BSA

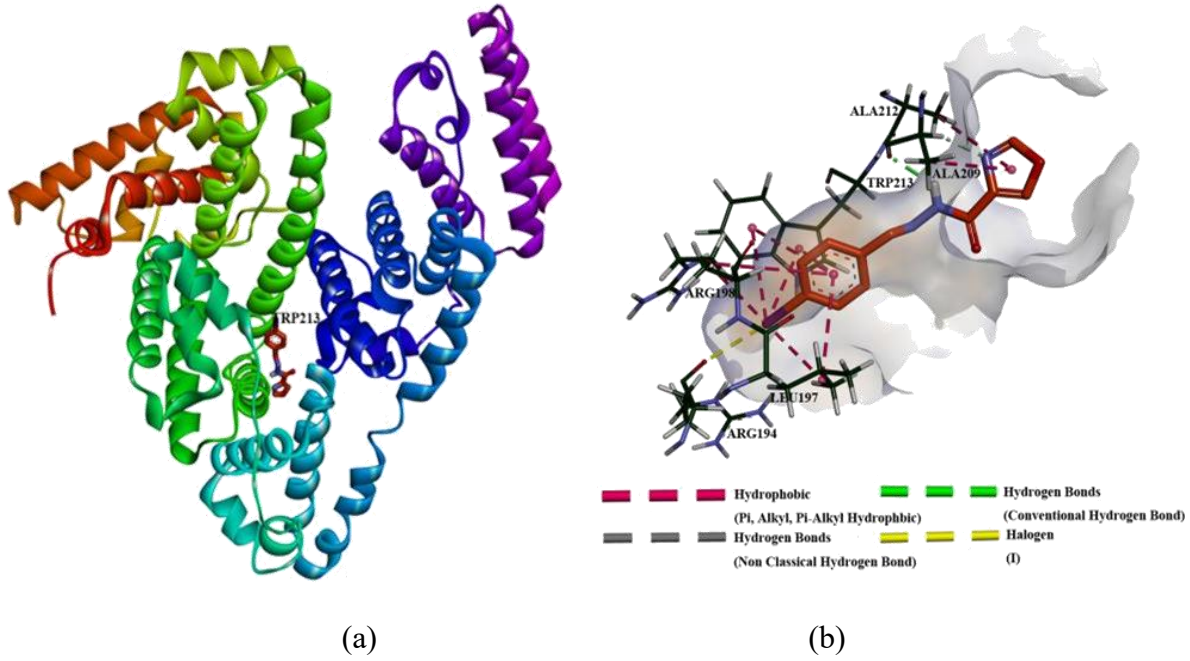

(a) (b)

Figure 15. Molecular docking result of **3** with BSA (a) The best docked pose of **3** in BSA (b) Detailed view of binding mode of **3** with BSA

Antioxidant studies

DPPH radical scavenging activities of **1-3** were shown in **Figure 16**. As presented in **Figure 16**, when the acylhydrazone was mixed with DPPH radical, the absorbance of DPPH radical was decreased at 517 nm. This was due to the scavenging effect of the amino groups for **1-3** on DPPH radicals. With increasing of acylhydrazone concentrations, the reactivity of DPPH radical was increased. The IC_{50} values of **1-3** were 96.31, 52.32, and 8.58 mg·mL^{-1}, respectively, indicating that the scavenging activity of **3** was the highest. The differences of antioxidant activities of **1-3** may be attributed to the redox properties of three acylhydrazones.

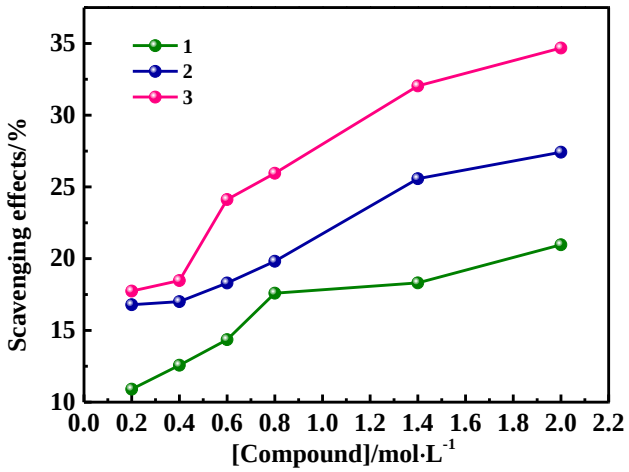

Figure 16. DPPH radical scavenging activities of **1-3**

Antibacterial activities

The antibacterial activities of **1-3** against *E. coli*, *S. aureus*, *B. subtilis*, and *P. aeruginosa* were measured by diffusion agar test. Supplementary **Figure S4** showed the diagrams of inhibtion zones of DMSO, streptomycin sulfate, **1**, **2**, and **3** against four kinds of bacteria. The average diameters (mm) of inhibition zones were presented in **Table 8**. It was found that DMSO had no effect on the four kinds of bacteria, while the control drug streptomycin sulfate (2.0 mg·mL^{-1}) had strong antibacterial activities to all bacteria. The antibacterial activity of **1** against *P. aeruginosa* (13.34 mm) was strongest, followed by *B. subtilis* (11.96 mm), and then *E. coli* (10.28 mm), and the last *S. aureus* (10.25 mm). However, the antibacterial activities of **1** against four kinds of bacteria were all weaker than streptomycin sulfate. The order of antibacterial activity of **2** against four kinds of bacteria was as follows: *E. coli* (10.98 mm), *P. aeruginosa* (10.86 mm), *B. subtilis* (10.44 mm), and *S. aureus* (10.36 mm). For **3**, it had the greatest effect on *B. subtilis* (13.83 mm), followed by *P. aeruginosa* (10.80 mm), and then *S. aureus* (10.35 mm), while the antibacterial activity of **3** against *E. coli* was weaker than others. It's remarkable that with the decreasing of acylhydrazone concentrations, the inhibition zones of **1-3** were also decreased. And when the concentrations were decreased to 0.25 mg·mL^{-1}, the average diameters of inhibition zones of **1-3** against four kinds of bacteria were similar to that of DMSO (blank control). These results revealed that the minimum inhibitory concentrations (MICs) of **1-3** against four kinds of bacteria were all 0.25 mg·mL^{-1}.

Table 8. The antibacterial zone diameters of **1-3**, DMSO and streptomycin sulfate

Compound		Antibacterial zone diameter (mm)			
		Escherichia coli (A)	*Staphylococcus aureus* (B)	*Bacillus subtilis* (C)	*Pseudomonas aeruginosa* (D)
DMSO		8.09 (A11)	7.76 (B11)	7.68 (C11)	7.68 (D11)
Streptomycin sulfate		17.16 (A21)	12.48 (B21)	13.18 (C21)	15.33 (D21)
2.00 mg·mL^{-1}	**1**	10.28 (A31)	10.25 (B31)	11.96 (C31)	13.34 (D31)
	2	10.98 (A41)	10.36 (B41)	10.44 (C41)	10.86 (D41)
	3	9.78 (A51)	10.35 (B51)	13.83 (C51)	10.80 (D51)
1.00 mg·mL^{-1}	**1**	9.86 (A32)	9.31 (B32)	9.85 (C32)	9.23 (D32)
	2	9.83 (A42)	9.40 (B42)	9.26 (C42)	9.29 (D42)
	3	9.48 (A52)	10.23 (B52)	9.35 (C52)	10.17 (D52)
0.50 mg·mL^{-1}	**1**	9.12 (A33)	8.82 (B33)	9.20 (C33)	8.52 (D33)
	2	8.98 (A43)	9.05 (B43)	8.38 (C43)	9.06 (D43)
	3	8.61 (A53)	9.47 (B53)	8.91 (C53)	9.49 (D53)
0.25 mg·mL^{-1}	**1**	7.85 (A34)	8.28 (B34)	8.34 (C34)	6.89 (D34)
	2	7.13 (A44)	8.59 (B44)	7.71 (C44)	8.48 (D44)
	3	8.51 (A54)	9.15 (B54)	8.11 (C54)	8.34 (D54)

CONCLUSION

Three acylhydrazones containing oxazole ring named **1**, **2**, and **3** have been synthesized by the condensation reactions of the 4-oxazolecarboxylic acid hydrazide with benzaldehyde containing halogen atoms in EtOH. The single crystal XRD indicated that **1** belonged to the monoclinic system and $P2_1$ space group, while **2** and **3** belonged to the triclinic systems and *P*1 and *P*-1 space groups. TG-DTG results

illustrated that **1** was the stablest. CT-DNA binding studies indicated that the mode of interaction between each acylhydrazone and CT-DNA was groove binding and the order of their binding constants was **2**>**1**>**3**. BSA binding studies revealed that each acylhydrazone reacted with BSA to form a complex by static quenching effect. Microcalorimetry measurements illustrated the interaction processes of **1**-**3** with CT-DNA/BSA were all exothermic. The molecular docking results confirmed the binding modes between acylhydrazones and CT-DNA/BSA. Antioxidant studies of **1**-**3** showed that the order of radical scavenging activities was **3>2>1**. Antibacterial experiments illustrated that **3** exhibited the strongest inhibition activity against *Bacillus subtilis* at the concentration of 2.00 $mg \cdot mL^{-1}$. In conclusion, we found that three acylhydrazones containing oxazole ring had strong biological activities after various physical and biological evaluations, which were expected to be candidate pharmaceutical for pharmaceutical intermediates.

EXPERIMENTAL

Chemicals and methods

Hydrazine hydrate (80%), ethanol (EtOH), methanol (MeOH), and DMSO were purchased from Fuyu Fine Chemical Industry. Ethyl oxazole-4-carboxylate was obtained from Bide Pharmatech Co., Ltd. 4-fluorobenzaldehyde, 4-bromobenzaldehyde, and 4-iodobenzaldehyde were purchased from Yingrui Chemical Technology Co., Ltd. BSA and CT-DNA were obtained from Bailingwei Co., Ltd and Sigma Aldrich, respectively. *E. coli*, *S. aureus*, *B. subtilis*, and *P. aeruginosa* were purchased from China Center of Industrial Culture Collection (CICC). All chemicals were obtained from commercial sources and used without further purification.

The melting points were measured by WRS-2U micro melting point tester. Elemental analyses were obtained using a P.E.2400-II instrument. Infrared spectra were measured by a Bruker Tensor-II Fourier infrared spectrometer. The ^1H NMR spectra were recorded on a Bruker Avance DRX-400 NMR spectrometer. The single crystal XRD were determined using a Bruker smart apex II CCD diffractometer. The thermal stabilities were determined by TG-DSC1 HT thermogravimetric analyzer. UV-vis spectra were studied by a TU-1950 UV spectrophotometer. Viscosity measurements were investigated by a Ubbelohde viscometer. Fluorescence spectra were carried out by LS55 (λ_{ex} = 280 nm) fluorescence spectrometer and the thermogenic curves were measured by C80 microcalorimeter.

Synthesis of $[C_4N_4O_2H_5]$

According to the reference,[30] firstly, ethyl oxazole-4-carboxylate (1.4113 g, 10.0 mmol) was dissolved in EtOH (15 mL), then hydrazine hydrate (3 mL, 80%) was added in the above solution. The mixture was stirred in a water bath at 25 °C for 1 h. The white flocs were obtained after the mixture standing for 1 day

at rt. The white flocs of 4-oxazolecarboxylic acid hydrazide were collected and washed three times with EtOH. Yield: 85.2%, mp 247.61-248.71 °C; Anal. Calcd for $C_4H_5N_3O_2$ (%): C, 36.97; H, 3.89; N, 33.15; Found (%): C, 37.20; H, 3.97; N, 33.06. IR (KBr, cm^{-1}) *v*: 1688 (C=O), 1331 (C-N), 1582 (C=N). ^{1}H NMR (400 MHz, DMSO-d_6): δ (ppm) = 9.54 (s, 1H, NH), 8.60 (s, 1H, oxazole-H), 8.49 (s, 1H, oxazole-H), 4.47 (s, 2H, NH2).

Syntheses of 1-3

4-Oxazolecarboxylic acid hydrazide (0.1411 g, 1.0 mmol) was dissolved in 50 mL EtOH, and then 4-fluorobenzaldehyde (120 μL, 1.0 mmol) was added. The mixture was refluxed with stirring at 75 °C for 4 h. The colorless of crystals 4-oxazolecarboxylic acid 2-(4-fluorophenyl)methylenehydrazide (**1**) were obtained after standing for 2 days at room temperature. The colorless crystals were collected and washed three times with EtOH. Yield: 78.8%, mp 212.68-213.18 °C, Anal. Calcd for $C_{11}H_8N_3O_2F$ (**1**, %): C, 56.42; H, 3.18; N, 17.63; Found (%): C, 56.66; H, 3.16; N, 18.02. IR (KBr, cm^{-1}) ν: 1676 (C=O), 1607 (C=N) imine, 1576 (C=N) oxazole, 1238 (C-F). ^{1}H NMR (400 MHz, DMSO-d_6): δ (ppm) = 11.89 (s, 1H, NH), 8.83 (d, J = 1.0 Hz, 1H, CH), 8.63 (d, J = 0.9 Hz, 1H, oxazole-H), 8.49 (s, 1H, oxazole-H), 7.87-7.79 (m, 2H, Ar-H), 7.50 (dd, J = 8.7, 2.2 Hz, 2H, Ar-H).

Colorless crystals of 4-oxazolecarboxylic acid 2-(4-bromophenyl)methylenehydrazide (**2**) were prepared by adopting the similar procedure used for synthesis of **1** but using 4-bromobenzaldehyde (0.1850 g, 1.0 mmol) instead of 4-fluorobenzaldehyde (120 μL, 1.0 mmol). Yield: 84.8%, mp 268.60-269.60 °C, Anal. Calcd for $C_{11}H_8N_3O_2Br$ (**2**, %): C, 53.76; H, 2.86; N, 16.56; Found (%): C, 53.72; H, 2.74; N, 16.29. IR (KBr, cm^{-1}) ν: 1670 (C=O), 1601 (C=N) imine, 1522 (C=N) oxazole, 630 (C-Br). ^{1}H NMR (400 MHz, DMSO-d_6): δ (ppm) = 11.90 (s, 1H, NH), 8.84 (d, J = 1.0 Hz, 1H, CH), 8.63 (d, J = 1.0 Hz, 1H, oxazole-H), 8.53 (s, 1H, oxazole-H), 7.66 (s, 4H, Ar-H).

Colorless crystals of 4-oxazolecarboxylic acid 2-(4-iodophenyl)methylenehydrazide (**3**) were obtained in the above similar way, except using 4-iodobenzaldehyde (0.2320 g, 1.0 mmol) instead of 4-fluorobenzaldehyde (120 μL, 1.0 mmol). Yield: 77.9%, mp 249.37-250.27 °C, Anal. Calcd for $C_{11}H_8N_3O_2I$ (**3**, %): C, 38.77; H, 2.37; N, 12.78; Found (%): C, 38.73; H, 2.36; N, 12.35. IR (KBr, cm^{-1}) ν: 1665 (C=O), 1597 (C=N) imine, 1566 (C=N) oxazole, 614 (C-I). ^{1}H NMR (400 MHz, DMSO-d_6): δ (ppm) = 11.83 (s, 1H, NH), 8.83 (d, J = 1.0 Hz, 1H, CH), 8.63 (d, J = 1.0 Hz, 1H, oxazole-H), 8.54 (s, 1H, oxazole-H), 7.88-7.70 (m, 2H, Ar-H), 7.37-7.19 (m, 2H, Ar-H).

X-Ray crystal structure determination of 1-3

Crystallographic data of **1-3** were performed at 293(2) K with graphite monochromated Mo-Kα radiation (λ = 0.071073 nm). The structures were solved using direct methods and refined using full-matrix

least-squares on F^2 with the SHELXL-97 program. All non-H atoms were refined anisotropically and the hydrogen atoms were placed at geometrically idealist positions and refined using a riding model.

Thermal stabilities of 1-3

The thermal decomposition processes of three acylhydrazones were investigated at heating rates of 5.00, 10.00 and 15.00 °C·min^{-1} from rt to 600.00 °C by thermogravimetric analyzer under the nitrogen atmosphere. The apparent activation energies (E_a) of the thermal decomposition stages of **1-3** were calculated by Kissinger and Ozawa methods. The formulas were as follows.[31]

$$\ln\left(\beta/T_p^{\,2}\right)=\ln\left(AR/E_a\right)-E_a/RT_p \qquad \text{(Kissinger)} \qquad (7)$$

$$\lg\beta=\lg\left[AE_a/RG(\alpha)\right]-2.315-0.4567\,E_a/RT_p \qquad \text{(Ozawa)} \qquad (8)$$

here T_p is the decomposition peak temperature value, A the pr-exponential factor, E_a the apparent activation energy, R the gas molar constant (8.314 J·mol^{-1}·K^{-1}), β the heating rate, and $G(\alpha)$ the integral mechanism function. For Kissinger equation, a plot of $\ln(\beta/T_p^2)$ versus $1/T_p$ gave a slope and the intercept equal to E_a/R and $\ln(AR/E_a)$, respectively. For Ozawa equation, a plot of $\lg\beta$ versus $1/T_p$ gave a slope and the intercept equal to $0.4567E_a/R$ and $\lg[AE_a/RG(\alpha)]$, respectively.

CT-DNA binding studies

UV-vis absorption assay

Tris-HCl buffer solution (0.01 mol·L^{-1}, pH = 7.9) was prepared by dissolving tris(hydroxymethyl)aminomethane (0.3028 g) and NaCl (0.1461 g) in distilled water, and then the CT-DNA solution was prepared by dissolving CT-DNA (0.0050 g) in Tris-HCl buffer solution (50 mL). The CT-DNA concentration was determined spectrophotometrically at 260 nm using molar extinction coefficient ε_{260} = 6600 mol^{-1}cm^{-1}.[32] Each acylhydrazone solution (1.0×10^{-4} mol·L^{-1}) was obtained by dissolving acylhydrazone in the mixture of dimethyl sulfoxide (DMSO) and Tris-HCl (v/v = 5:95, 25 mL). UV-vis absorption assay was performed by increasing the concentration of CT-DNA while keeping the concentration of the acylhydrazone, and spectra were recorded in the 200~500 nm range at rt.

Fluorescence quenching studies

Tris-HCl buffer solution (0.01 mol·L^{-1}, pH = 7.2) was obtained in the above similar way, except that the pH was 7.2. The mixture of EB-CT-DNA (2.2×10^{-5} mol·L^{-1}) was formed by dissolving EB (0.0032 g) and CT-DNA (0.005 g) in Tris-HCl buffer solution (50 mL) and placed at rt for 30 min. Fluorescence spectra were performed keeping the concentration of the acylhydrazone (2.2×10^{-4} mol·L^{-1}) while varying the concentration of EB-CT-DNA. The spectra were recorded from 450 nm to 750 nm at rt and the excitation wavelength was 500 nm.

Microcalorimetry measurements

Microcalorimetry is a high-accuracy tool used to study the thermodynamics and kinetics of biomacromolecules.[33] The interactions of acylhydrazones with CT-DNA were studied by microcalorimetry measurements. The concentrations of all substances were the same as those of UV-vis absorption assay. Tris-HCl buffer solution (1 mL) and acylhydrazone solution (1 mL) were added into the bottom of reference cell and sample cell of microcalorimeter, respectively, then CT-DNA solution (1 mL) was added into the upper of two cells. When the baseline was stable, the solutions in upper and bottom cells were mixed, and the heat flows of the reactions were recorded at 25 °C.

BSA binding studies

UV-vis absorption spectral studies

Tris-HCl buffer solution (0.01 mol·L^{-1}, pH = 7.9) and three acylhydrazone solutions (1.0×10^{-4} mol·L^{-1}) were used in UV-vis absorption spectral studies. BSA solution (1.0×10^{-7} mol·L^{-1}) was prepared by dissolving BSA in Tris-HCl buffer solution (50 mL). The BSA concentration was determined spectrophotometrically at 280 nm using molar extinction coefficient ε_{280} = 44300 mol^{-1}cm^{-1}.[34] Then acylhydrazone solution (50 μL for each time) was gradually dropped into the BSA solution and the mixed solution was scanned from 250 nm to 500 nm at rt.

Fluorescence quenching studies

The solution of BSA was obtained by dissolving BSA (0.0033 g) in Tris-HCl buffer solution (0.01 mol·L^{-1}, pH = 7.2, 50 mL). In this study, the interaction of each acylhydrazone with BSA was measured by fluorescence spectra keeping the concentration of BSA while gradually increasing the concentration of each acylhydrazone (50 μL for each time). The change in the fluorescence spectra was scanned from 300 nm to 540 nm at rt and the excitation wavelength was 280 nm.

Microcalorimetry measurements

The interactions of **1**-**3** with BSA were studied by microcalorimetry measurements. The concentrations of all substances were the same as those of UV-vis absorption spectral studies of BSA. The operation processes were similar to the microcalorimetry measurements of interactions between CT-DNA and acylhydrazones, except using BSA(1 mL) instead of CT-DNA(1 mL). The heat flows of the reactions were recorded at 25 °C.

Molecular docking studies

Molecular docking studies of **1**-**3** were carried out by using Auto dock 4.0 software and the docking method was semi-flexible docking. The crystal structures of DNA (PDB ID: 425D) and BSA (PDB ID:

4F5S) were taken from RCSB Protein Data Bank (http://www.rcsb.org/pdb). The crystal structure information of each acylhydrazone was obtained from the cif file. The water molecules in the proteins were cleaned and recorded PDB format by Autodock tools. Discovery Studio 4.5 was used to prepare the PDBQT formats of DNA, BSA, and acylhydrazones. The lowest energy conformation was selected as the binding mode due to the lowest energy position indicated the highest binding affinity. The visualization of docking results was realized by Pymol and Discovery Studio 4.5.

Antioxidant studies

The antioxidant activities of **1**-**3** were determined by DPPH radical scavenging assay. DPPH solution (200 μmol·L^{-1}) was obtained by dissolving DPPH (0.0079 g) in EtOH (100 mL). Each acylhydrazone solution (10 mg·mL^{-1}) was prepared, and then diluted to 2.0, 1.4, 0.8, 0.6, 0.4, 0.2 mg·mL^{-1}. The acylhydrazone solution (1 mL), EtOH (4 mL) and 200 μmol·L^{-1} DPPH (5 mL) were added into a 10 mL volumetric flask, making the final concentration of DPPH was 100 μmol·L^{-1}. The control group was DMSO instead of acylhydrazone solution and the mixture was evenly mixed and placed at rt for 20 min. The decrease in absorbance of DPPH was determined by UV-vis spectra at 517 nm. The percentage of scavenging activity was calculated using equation (9).[35]

$$\text{Scavenging activity (\%)} = (1 - A_x/A_0) \times 100\% \qquad (9)$$

Where A_0 is the absorbance of the control group, A_x the absorbance of DPPH with acylhydrazone.

Antibacterial experiments

The antibacterial activities of **1**, **2**, and **3** against *E. coli*, *S. aureus*, *B. subtilis*, and *P. aeruginosa* were studied by agar diffusion tests under strict aseptic conditions. Each acylhydrazone was dissolved in DMSO, and the final concentration was 2.0 mg·mL^{-1}. In the experiment, the concentration of each acylhydrazone was diluted by double dilution method to determine the minimum inhibitory concentration of each acylhydrazone. DMSO was used as blank control group and streptomycin sulfate (2.0 mg·mL^{-1}) as drug control group. The diameters (mm) of inhibition zones of three acylhydrazones were expressed in terms of the average diameters of inhibition zones.

ACKNOWLEDGEMENTS

This work was supported by the National Natural Science Foundation of China (Nos. U1903033, 21073139, 21373158) and Science and Technology on Combustion and Explosion Laboratory Foundation of Shaanxi (No. 6142603010301).

SUPPORTING INFORMATION

Supplementary (IR, ^{1}H NMR, cif and checkcif) data associated with this article can be found, in the

online version, at URL: https://www.heterocycles.jp/newlibrary/downloads/PDFsi/27023/102/1.

REFERENCES

1. R. M. Ramadan, A. K. A. Al-Nasr, and O. A. M. Ali, *J. Mol. Struct.*, 2018, **1161**, 100.
2. L. Q. Zhang, J. M. Liu, Y. Y. Gan, L. H. Shao, Y. H. Fu, Z. C. Wang, and G. P. Ouyang, *Heterocycles*, 2020, **100**, 1845.
3. M. Carcelli, D. Rogolino, A. Gatti, L. D. Luca, M. Sechi, G. Kumar, S. W. White, A. Stevaert, and L. Naesens, *Sci. Rep.*, 2016, **6**, 31500.
4. R. K. Gupta, G. Sharma, R. Pandey, A. Kumar, B. Koch, P. Z. Li, Q. Xu, and D. S. Pandey, *Inorg. Chem.*, 2013, **52**, 13984.
5. A. N. Aziz, M. Taha, N. Ismail, E. Anouar, S. Yousuf, W. Jamil, K. Awang, N. Ahmat, K. M. Khan, and S. M. Kashif, *Molecules*, 2014, **19**, 8414.
6. J. P. Rada revised manuscript.docx, B. S. M. Bastos, L. Anselmino, C. H. J. Franco, M. Lanznaster, R. Diniz, C. O. Fernández, M. M. Márquez, A. M. Percebom, and N. A. Rey, *Inorg. Chem.*, 2019, **58**, 8800.
7. R. Moreno-Fuquen, F. Cuenú, J. E. Torres, G. De la Vega, E. Galarza, R. Abonia, and A. R. Kennedy, *J. Mol. Struct.*, 2017, **1150**, 366.
8. S. Kotha and S. R. Cheekatla, *Heterocycles*, 2020, **100**, 1623.
9. H. Z. Zhang, L. L. Gan, H. Wang, and C. H. Zhou, *Mini-Rev. Med. Chem.*, 2017, **17**, 122.
10. X. M. Peng, G. X. Cai, and C. H. Zhou, *Curr. Top. Med. Chem.*, 2013, **13**, 1963.
11. I. Zahanich, I. Kondratov, V. Naumchyk, Y. Kheylik, M. Platonov, S. Zozulya, and M. Krasavin, *Bioorg. Med. Chem. Lett.*, 2015, **25**, 3105.
12. P. C. Patil, J. Tan, D. R. Demuth, and F. A. Luzzio, *Bioorg. Med. Chem.*, 2016, **24**, 5410.
13. E. Masumoto, H. Nagabuchi, N. Kashige, F. Okabe-Nakahara, F. Miake, K. Yamagata, and H. Maruoka, *Heterocycles*, 2019, **99**, 669.
14. S. Tabassum, M. Ahmad, M. Afzal, M. Zaki, and P. K. Bharadwaj, *J. Photochem. Photobiol. B*, 2014 **140**, 321.
15. P. Sathyadevi, P. Krishnamoorthy, M. Alagesan, K. Thanigaimani, P. T. Muthiah, and N. Dharmaraj, *Polyhedron*, 2012, **31**, 294.
16. (a) T. Sedaghat, M. Yousefi, G. Bruno, R. H. Amiri, H. Motamedi, and V. Nobakht, *Polyhedron*, 2014, **79**, 88; (b) D. Saha, T. Maity, T. Dey, and S. Koner, *Polyhedron*, 2012, **35**, 55.
17. X. L. Xing, F. Q. Zhao, S. N. Ma, S. Y. Xu, L. B. Xiao, H. X. Gao, and R. Z. Hu, *J. Therm. Anal. Calorim.*, 2012, **110**, 1451.
18. K. Liu, G. L. Chang, H. Yan, Z. Li, M. Hong, and M. J. Niu, *Inorg. Chim. Acta*, 2017, **464**, 137.

19. J. Eberhard, I. Stoll, R. Brockhinke, B. Neumann, H. G. Stammler, A. Riefer, E. Rauls, W. G. Schmidtd, and J. Mattayand, *CrystEngComm*, 2013, **15**, 4225.
20. (a) R. K. Thomas, S. Sukumaran, and C. Sudarsanakumar, *J. Mol. Struct*., 2019, **1178**, 62; (b) S. Bi, H. Zhou, J. Wu, and X. Y. Sun, *J. Biomol. Struct. Dyn*., 2019, **37**, 1464.
21. X. Feng, Y. Wu, Q. Zhang, and J. C. Liu, *Dyes Pigm*., 2017, **161**, 115.
22. N. Wang, L. Ye, B. Q. Zhao, and J. X. Yu, *J. Med. Biol. Res*., 2008, **41**, 589.
23. H. Y. Liu, Z. H. Xu, X. H. Liu, P. X. Xi, and Z. Z. Zeng, *Chem. Pharm. Bull*., 2009, **57**, 1237.
24. M. V. D. Weert and L. Stella, *J. Mol. Struct*., 2011, **998**, 144.
25. J. R. Lakowicz, In 'Principles of Fluorescence Spectroscopy' 3rd ed, Springer, New York, 2006.
26. (a) X. Feng, Y. Wu, Q. Zhang, and J. C. Liu, *Dyes Pigm*., 2017, **161**, 115; (b) E. Ciotta, P. Prosposito, and R. Pizzoferrato, *J. Lumin*., 2019, **206**, 518.
27. G. Kalaiarasi, C. Umadevi, A. Shanmugapriya, P. Kalaivani, F. Dallemer, and R. Prabhakaran, *Inorg. Chim. Acta*, 2016, **453**, 547.
28. X. J. Zong, X. R. Liu, S. S. Zhao, and Z. W. Yang, *Polyhedron*, 2019, **170**, 303.
29. A. Sulkowska, *J. Mol. Struct*., 2002, **614**, 227.
30. H. Tang, Y. X. Jin, and F. Y. Pan, *Sci. Tech. Engng*., 2007, **7**, 2934.
31. H. Derakhshankhah, A. A. Saboury, A. Divsalar, and H. Mansouri-Torshizi, *Biophys. J*., 2011, **100**, 217a.
32. C. J. Baltazar, R. Mun, and H. A. Tajmir-Riahi, and J. Bariyanga, *J. Mol. Struct*., 2018, **1161**, 273.
33. (a) Y. Feng, Y. Liu, C. L. Xie, S. S. Qu, Z. F. Le, H. Y. Sheng, M. S. Duan, and X. C. Zhang, *Thermochim. Acta*, 1996, **285**, 181; (b) Y. Liang, C. X. Wang, G. L. Zou, Z. Y. Wang, Y. W. Liu, and S. S. Qu, *Thermochim. Acta*, 2000, **351**, 21; (c) W. Yu, S. Lei, G. Hui, and F. Cui, *J. Lumin*., 2013, **134**, 491.
34. A. Ray, B. K. Seth, U. Pal, and S. Basu, *Spectrochim. Acta, Part A*, 2012, **92**, 164.
35. J. C. Wang, G. S. Xing, W. D. Hu, T. L. Zhu, Q. Wang, and H. Zhao, *Chinese Pharm. J.*, 1994, **29**, 23.